Electronic Supplementary Material (ESI) for Journal of Materials Chemistry A.

Supporting Information

Descriptor of Catalytic Activity of Metal Sulfides for Oxygen Reduction Reaction: A Potential Indicator for Mineral Flotation

Hongbiao Tao, Subiao Liu, Jing-Li Luo, Phillip Choi, Qi Liu*, Zhenghe Xu*

Department of Chemical and Materials Engineering, University of Alberta, Edmonton, Alberta T6G 1H9, Canada

Corresponding authors: Zhenghe Xu, Qi Liu

Telephone: +1 780 492-7667, +1 780 492-8628

*E-mail: Zhenghe.xu@ualberta.ca, qliu@ualberta.ca

Supporting Information contains:

S1. DFT Calculations

The Vienna *ab initio* Simulation Package (VASP)[1–4] with the projector-augmented plane-wave (PAW) method[5,6] was performed for the first-principle calculations in this study. The electron wavefunctions were presented by the planewave basis set and the cutoff energy for plane-wave basis functions was set at 450 eV. For all calculations, the spin polarization was enabled. For adsorption models of the oxygen reduction reaction (ORR) intermediates over the representative metal sulfides (i.e., Pt, FeS_2, $CuFeS_2$, PbS, ZnS), the revised Perdew-Burke-Ernzerhof (RPBE) generalized gradient approximation functional (GGA)[7] was adopted to describe the exchange and correlation interactions. The occupancy of the one-electron states was calculated using an electronic temperature of k_BT = 0.05 eV for surfaces and 0.01 eV for molecules in vacuum. All energies were extrapolated to T = 0 K. The slab models of Pt(111), FeS_2(100), $CuFeS_2$(112), PbS(100) and ZnS(110) comprising four, nine, six, six and six atomic layers, respectively, and the vacuum layer with thickness of 20 Å. The cleavage planes of (111), (100), (112), (100) and (110) were adopted for Pt,[8,9] FeS_2,[10] $CuFeS_2$,[11] PbS[12] and ZnS,[13] respectively, because they have been considered as stable and easily exposed planes, which have been extensively used as the model surfaces. We subsequently built the relevant ORR models with the metallic cations on the surface as the active center, attempting to understand the distinct activities of these materials for ORR. Meanwhile, the surface models were built with similar side lengths and contain eight metallic sites on the surface to guarantee the intermediate coverage of 1/8 ML. During the geometry optimization of the slab models, half of the bottom atomic layers were constraint, while other layers were relaxed. The structures were geometrically optimized until the force components were less than 0.05 eV/Å. The similar density of Monkhorst-Pack k-point grids[14] (i.e., 7×7×7 for unit cell of

galena) was set to sample the Brillouin zone for all the surface models, while only the Gamma point was included for molecules.

Given that metal sulfides present different crystal structures and contain various metallic cations, different GGA functionals were tested for full optimization of the unit cells before calculating the bulk descriptor (i.e., the bulk centroid of the occupied S 3p band relative to the Fermi level). The experimental lattice constants and the lattice constants calculated with different GGA functionals are listed in Table S1. It shows that DFT calculations with the GGA_PBE functional reproduced experimental crystal structures better than the results obtained with other GGA functionals. However, even crystal structures optimized with the GGA_PBE functional present various levels of discrepancies. Therefore, we calculated the electronic structures for internally optimized crystals using the GGA_PBE functional, as enlightened by previous research on perovskite.[15] Moreover, the surface descriptors were also calculated for metal sulfides possessing ideal cleavage planes. The surface models were built directly with the internally optimized structures of the unit cells and then optimized in the same way as that for the ORR models. The descriptor was calculated for sulfur anions on the first layer of the surface and was shown in Figure 3(c). The descriptor was determined by taking the centroid of the occupied projected density of states of the sulfur p states or metal d states relative to the Fermi level using the commonly used formula,[16–19]

$$band\ center = \frac{\int E \cdot f(E) dE}{\int f(E) dE}$$

Where E is the electron energy, $f(E)$ is the corresponding PDOS value.

Regarding the chemisorption of the atomic oxygen, we also calculated the oxygen binding strength on the typical sulfur site on the surface. The calculated oxygen chemisorption energy on the sulfur sites is compared with that on the metallic cation sites in Figure S1.

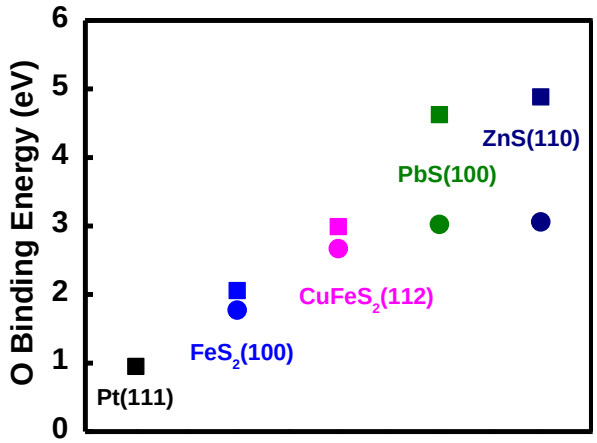

Figure S1. Oxygen binding energy on metal sites (Square) and sulfur sites (Circle)

In Figure S1, smaller values of the O binding energy indicate stronger chemisorption of oxygen on the surface. The relative oxygen chemisorption energies reflect the different levels of competitive adsorption of oxygen on the sulfur sites with that of the metal sites on the surface. It is noteworthy that oxygen binds much more strongly on the sulfur sites than that on the metal sites on the PbS and ZnS surfaces, which exhibit very poor catalytic activities for the ORR. The substantially stronger tendency of the adsorption of oxygen on the sulfur sites on surface of PbS and ZnS, as compared to those of FeS_2 and $CuFeS_2$, further highlights the dominating role of the metallic cations on the catalytic activity of metal sulfides for the ORR. Moreover, the consideration of choosing metallic cation as the active centers to build ORR models is based on previous experimental and theoretical studies.[15,20–27] Therefore, we believe that the selection of metallic cations as the active center to study the activity of metal sulfides for the ORR is reasonable and persuasive, as also supported by the established descriptor–activity relationship in our work.

In our study, we calculated both the occupied bulk metal d-band center and the bulk S p-band center. The correlation between the rest potential and the bulk d-band center is shown in Figure S2. As seen, the experimental rest potential exhibits a much better correlation with the bulk S p-band center with a coefficient of determination (i.e., R^2) of 0.88 as compared to that with the bulk

d-band center (R^2=0.71). Therefore, the sulfur p-band center was selected to the build the descriptor–activity relationship.

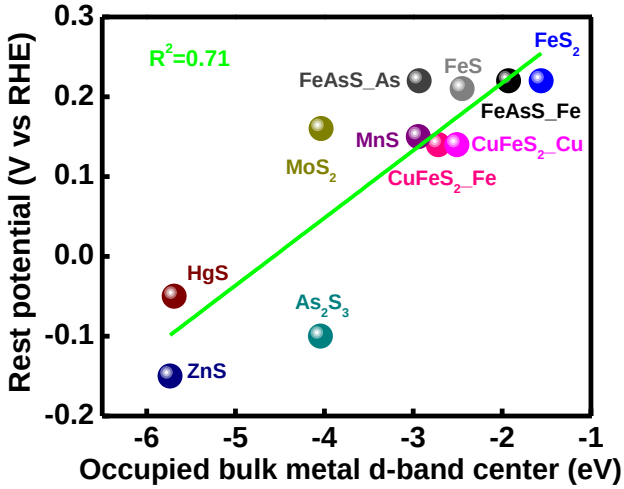

Figure S2. The experimental rest potentials plotted against the occupied bulk metal d-band center relative to the Fermi energy. The d-band center of galena is – 16.84 which is not included in this plot.

S2. Gibbs free energy diagram

Gibbs free energy diagram for ORR was constructed through thermodynamically corrected DFT calculation results in combination with the computational hydrogen electrode (CHE) model where each electrochemical reaction step is treated as a simultaneous transfer of the proton-electron pair as a function of the applied potential.[7,28] The associative model was adopted for the ORR,[25]

$$4H^+ + 4e + O_2 + *$$
$$\downarrow$$
$$3H^+ + 3e + OOH/*$$
$$\downarrow$$
$$2H^+ + 2e + H_2O + O/*$$
$$\downarrow$$
$$H^+ + e + H_2O + OH/*$$
$$\downarrow$$
$$2H_2O + *$$

where * indicates the underlying surface. Using the final state where two gaseous water molecules freely above an empty surface as the reference, the Gibbs free energies of each elementary step were represented as,

$$G[0] = G[O_2] + 4G[H^+ + e^-] + G[*] - (G[*] + 2G[H_2O]) \quad (1)$$

$$G[1] = G[OOH^*] + 3G[H^+ + e^-] - (G[*] + 2G[H_2O]) \quad (2)$$

$$G[2] = G[O^*] + 2G[H^+ + e^-] - (G[*] + G[H_2O]) \quad (3)$$

$$G[3] = G[OH^*] + G[H^+ + e^-] - (G[*] + G[H_2O]) \quad (4)$$

$$G[5] = 0 \quad (5)$$

The free energies for relevant species were then calculated with the expression,

$$G = E_{DFT} + E_{ZPE} + \int C_p dT - TS + E_w \quad (6)$$

where E_{DFT} is the DFT calculated electronic energy with VASP; E_{ZPE} is the zero-point vibrational energy; $\int C_p dT$ is the enthalpy correction; TS is the entropy contribution and E_w is the stabilization of water molecules on the adsorbed intermediates which were obtained from the previous researches on platinum and metal sulfides for ORR.[8,29,30] In their studies, ice-like water bilayer structure on the surface was constructed, where half of the water molecules are $* H_2O$ and the other half have an O-H bond pointing down, as proposed by H. Ogasawara et al. and S. Maier et al.[31,32]

S3. Thermodynamic corrections

To construct the Gibbs free energy diagram, the DFT calculated electronic energies were corrected with contributions to thermodynamic quantities from translational, electronic, rotational and

vibrational motions. The contributions to entropy and enthalpy from different components were calculated with the standard methods.[33] The basic ideas and equations used for relevant calculations will be briefly introduced in this section, more details can go to the reference. For non-adsorbed molecules, the standard ideal gas methods were employed, where the contributions to enthalpy and entropy are calculated as,[33,34]

$$H(T) = E_{DFT} + E_{ZPE} + \int_0^{298.15} C_p dT \tag{7}$$

$$C_p = C_{V,trans} + C_{V,rot} + C_{V,vib} + C_{V,elec} + k_B \tag{8}$$

$$S(T,P) = S(T,P^0) - k_B ln\frac{P}{P^0} = S_{trans} + S_{rot} + S_{elec} + S_{vib} + k_B ln\frac{P}{P^0} \tag{9}$$

Where $H(T)$ is the ideal-gas enthalpy; C_p is the constant-pressure heat capacity; C_V is the constant-volume heat capacity which is separated into translational ($C_{V,trans}$), rotational ($C_{V,rot}$), vibrational ($C_{V,vib}$) and electronic ($C_{V,elec}$) parts. The translational heat capacity is $1.5k_B$ for a three-dimensional gas; the rotational heat capacity is k_B for linear molecule and $1.5k_B$ for nonlinear molecule; the electronic heat capacity is assumed to be 0. $S(T,P)$is the ideal-gas entropy comprising contributions from the four components. The equations for the integrated vibrational heat capacity and different contributions to the entropy are expressed as,

$$\int_0^T C_{V,vib} dT = \sum_i^{\mathrm{DOF}} \frac{hw_i}{e^{hw_i/k_BT}-1} \tag{10}$$

$$S_{trans} = k_B\{ln[(\frac{2\pi M k_B T}{h^2})^{3/2}\frac{k_B T}{P^0}] + \frac{5}{2}\} \tag{11}$$

$$S_{rot} = k_B\{\ln\left[\frac{\sqrt{\pi I_A I_B I_C}}{\sigma}\left(\frac{8\pi^2 k_B T}{h^2}\right)^{\frac{3}{2}}\right] + \frac{3}{2}\} \quad \text{for non-linear molecule} \tag{12}$$

$$= k_B\left[ln\left(\frac{8\pi^2 I k_B T}{\sigma h^2}\right) + 1\right] \quad \text{for linear molecule} \tag{13}$$

$$S_{vib} = k_B \sum_i^{\mathrm{DOF}} [\frac{hw_i}{k_B T(e^{hw_i/k_B T}-1)} - \ln(1 - e^{-\frac{hw_i}{k_B T}})] \quad (14)$$

$$S_{elec} = k_B \ln[2S + 1] \quad (15)$$

Where M is the molecular weight, w_i is the vibrational frequency, h is the Planck constant, k_B is the Boltzmann constant, I is the moment inertia, σ is the symmetry number of the molecule, S is the spin multiplicity, DOF indicates the degree of freedom which is $3N - 5$ for linear molecule and $3N - 6$ for non-linear molecule, N is the number of atoms in the molecule.

For adsorbed molecules on the surface, the harmonic limit method was adopted. Within this scheme, the harmonic approximation where all $3N$ degrees of freedom were treated as frustrated harmonic vibrations was used to treat the adsorbates, with negligible contributions from the underlying surfaces, and the PV contributions were neglected. Thus, the enthalpy and entropy of the adsorbate are calculated as,

$$H(T) = E_{DFT} + E_{ZPE} + \sum_i^{3N} \frac{hw_i}{e^{hw_i/k_B T}-1} \quad (16)$$

$$S(T) = S_{vib} = k_B \sum_i^{3N} [\frac{hw_i}{k_B T(e^{hw_i/k_B T}-1)} - ln(1 - e^{-\frac{hw_i}{k_B T}})] \quad (17)$$

The entropy of H_2O is calculated at 0.035 bar, corresponding to the equilibrium pressure of H_2O at room temperature, and the free energy of this state is therefore equal to that of liquid water. Furthermore, within the CHE model,[8] the free energy of the proton-electron pair is related to that of the gaseous hydrogen molecule under standard conditions,

$$G[H^+(aq) + e^-] = G[{}^1/_2\, H_2(g)] \quad (18)$$

Since pH in the practical electrochemical system is not 0, the reversible hydrogen electrode (RHE) is adopted. The difference between the SHE and RHE scales corresponds to the free energy difference of going from $pH = 0$ to a different pH, where the free energy of hydrogen ion is corrected with $G(pH) = k_B T ln(a_{H^+}) = -k_B T(ln10)pH$. Considering that the free energy trend of different elementary steps is not affected by the pH value, and the experimental catalytic activity trend for ORR of the representative materials remains the same in both acidic and alkaline conditions,[35] for simplicity, the pH value was set as 0. At a different electrode potential U, the Gibbs free energy for all states are shifted down by $-eU$. The effect of the external potential on the adsorbed intermediate was neglected due to the relatively small corrections as shown by previous research.[8,29] The chemical potential of the proton-electron pair can thus be expressed as,

$$G[H^+(aq)] + e^-] = G\left[{}^1/_2\, H_2(g)\right]) - eU \tag{19}$$

The atomic oxygen binding energy (ΔE_O) was calculated as the reaction energy,[25]

$$\Delta E_O = E_{surface/O} + E_{H_2} - E_{surface} - E_{H_2O} \tag{20}$$

where $E_{surface/O}$ and $E_{surface}$ are the DFT calculated electronic energies of the slab with and without adsorbed O, respectively. E_{H_2O} and E_{H_2} are the gas phase energies of water and hydrogen molecule, respectively. All the relevant thermodynamic data calculated for construction of the Gibbs free energy diagrams is listed in Table S2.

Table S1. Experimental crystal structures of sulfide minerals[36] and the DFT optimized crystal structures with different GGA functionals implemented in VASP

Sulfides	Experimental (Å)			Functional	Optimized (Å)			Δ (%)		
	a	b	c		a	b	c	a	b	c
Alabandite	5.225	5.225	5.225	PW91	5.117	5.117	5.117	-2.051	-2.051	-2.051
Mn_4S_4				PBE	5.126	5.126	5.126	-1.880	-1.880	-1.880
				PBEsol	5.117	5.117	5.117	-2.051	-2.051	-2.051
				RPBE	5.090	5.090	5.090	-2.569	-2.569	-2.569
Arsenopyrite	5.744	5.675	5.785	PW91	5.749	5.673	5.765	0.084	-0.027	-0.342
$Fe_4As_4S_4$				PBE	5.742	5.671	5.761	-0.028	-0.075	-0.413
				PBEsol	5.663	5.595	5.687	-1.409	-1.411	-1.690
				RPBE	5.765	5.693	5.783	0.366	0.309	-0.034
Chalcopyrite	5.290	5.290	10.422	PW91	5.276	5.276	10.179	-0.267	-0.267	-2.330
$Cu_4Fe_4S_8$				PBE	5.288	5.288	10.296	-0.041	-0.041	-1.208
				PBEsol	5.048	5.048	9.930	-4.573	-4.573	-4.715
				RPBE	5.358	5.358	10.576	1.286	1.286	1.476
Cinnabar	4.150	4.150	9.510	PW91	3.952	3.952	9.669	-4.759	-4.759	1.670
Hg_3S_3				PBE	3.948	3.948	9.668	-4.873	-4.873	1.662
				PBEsol	3.867	3.867	9.471	-6.823	-6.823	-0.405
				RPBE	3.999	3.999	9.764	-3.644	-3.644	2.673
Galena	5.936	5.936	5.936	PW91	6.005	6.005	6.005	1.166	1.166	1.166
Pb_4S_4				PBE	6.008	6.008	6.008	1.207	1.207	1.207
				PBEsol	5.900	5.900	5.900	-0.603	-0.603	-0.603
				RPBE	6.072	6.072	6.072	2.280	2.280	2.280
Molybdenite	3.161	3.161	12.295	PW91	3.197	3.197	14.044	1.133	1.133	14.228
Mo_2S_4				PBE	3.190	3.190	14.389	0.910	0.910	17.032
				PBEsol	3.147	3.147	12.566	-0.444	-0.444	2.208
				RPBE	3.208	3.208	14.690	1.478	1.478	19.476
Orpiment	11.475	9.577	4.256	PW91	11.426	10.875	4.557	-0.431	13.554	7.077
As_2S_3				PBE	11.414	10.975	4.578	-0.531	14.600	7.575
				PBEsol	11.507	9.500	4.049	0.281	-0.804	-4.870
				RPBE	11.459	12.029	5.013	-0.142	25.608	17.776
Pyrite	5.417	5.417	5.417	PW91	5.415	5.415	5.415	-0.039	-0.039	-0.039
Fe_4S_8				PBE	5.408	5.408	5.408	-0.167	-0.167	-0.167
				PBEsol	5.329	5.329	5.329	-1.616	-1.616	-1.616
				RPBE	5.440	5.440	5.440	0.427	0.427	0.427
Sphalerite	5.409	5.409	5.409	PW91	5.451	5.451	5.451	0.779	0.779	0.779

Zn_4S_4				PBE	5.448	5.448	5.448	0.715	0.715	0.715
				PBEsol	5.367	5.367	5.367	-0.777	-0.777	-0.777
				RPBE	5.538	5.538	5.538	2.374	2.374	2.374
Stibnite	11.282	3.830	11.225	PW91	11.916	3.876	11.281	5.621	1.218	0.501
Sb_2S_3				PBE	12.098	3.872	11.252	7.234	1.111	0.237
				PBEsol	11.278	3.829	10.909	-0.036	-0.014	-2.814
				RPBE	13.969	3.882	11.860	23.818	1.372	5.660
Troilite	5.965	5.965	11.757	PW91	5.843	5.843	10.452	-2.053	-2.053	-11.099
$Fe_{12}S_{12}$				PBE	5.835	5.835	10.433	-2.173	-2.173	-11.264
				PBEsol	5.711	5.711	10.304	-4.251	-4.251	-12.356
				RPBE	5.944	5.944	10.848	-0.354	-0.354	-7.731

Table S2. Thermodynamic corrections for molecules and ORR intermediates adsorbed on Pt(111), FeS_2(100), PbS(100),ZnS(110), $CuFeS_2$(112)_Fe and $CuFeS_2$(112)_Cu

Species/Adsorbate	Pressure (Pa)	E_{ZPE} (eV)	$\int C_p dT$ (eV)	− TS (eV)	$G - E_{DFT}$ (eV)
H_2	101325	0.279	0.090	-0.462	-0.093
H_2O	3500	0.566	0.104	-0.673	-0.003
O_2	101325	0.101	0.123	-0.563	-0.339
Pt111					0.000
*O		0.067	0.034	-0.061	0.040
*OH		0.356	0.048	-0.084	0.320
*OOH		0.426	0.100	-0.229	0.297
Pyrite100					0.000
*O		0.067	0.034	-0.061	0.040
*OH		0.348	0.054	-0.095	0.307
*OOH		0.403	0.109	-0.225	0.287
Galena100					0.000
*O		0.033	0.051	-0.109	-0.025
*OH		0.322	0.067	-0.134	0.255
*OOH		0.410	0.113	-0.254	0.269
Sphalerite110					0.000
*O		0.032	0.053	-0.129	-0.044
*OH		0.323	0.068	-0.143	0.248
*OOH		0.417	0.097	-0.217	0.297
Chalcopyrite112_Fe					0.000
*O		0.038	0.051	-0.151	-0.061
*OH		0.329	0.068	-0.162	0.235
*OOH		0.429	0.100	-0.206	0.323
Chalcopyrite112_Cu					0.000
*O		0.057	0.044	-0.101	0.000
*OH		0.334	0.062	-0.137	0.259
*OOH		0.423	0.106	-0.295	0.234

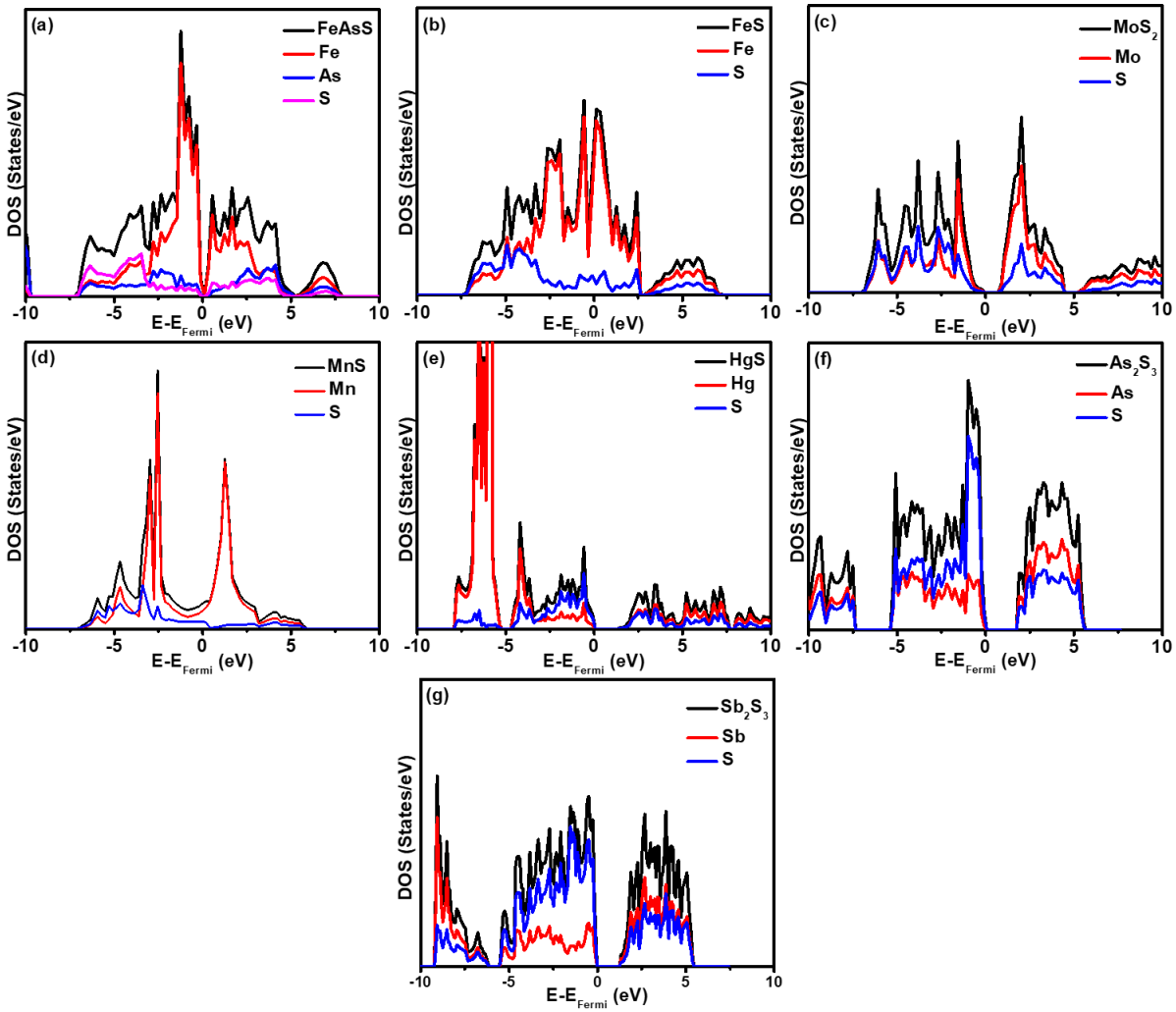

Figure S3. DFT calculated PDOS for bulk crystals: (a) FeAsS, (b) FeS, (c) MoS_2, (d) MnS, (e) HgS, (f) As_2S_3 and (g) Sb_2S_3

REFERENCES

1 G. Kresse and J. Hafner, *Phys. Rev. B*, 1993, **47**, 558–561.

2 G. Kresse and J. Hafner, *Phys. Rev. B*, 1994, **49**, 14251–14269.

3 G. Kresse and J. Furthmüller, *Comput. Mater. Sci.*, 1996, **6**, 15–50.

4 G. Kresse and J. Furthmüller, *Phys. Rev. B*, 1996, **54**, 11169–11186.

5 P. E. Blöchl, *Phys. Rev. B*, 1994, **50**, 17953–17979.

6 G. Kresse, *Phys. Rev. B*, 1999, **59**, 1758–1775.

7 B. Hammer, L. B. Hansen and J. K. Nørskov, *Phys. Rev. B*, 1999, **59**, 7413–7421.

8 J. K. Nørskov, J. Rossmeisl, A. Logadottir, L. Lindqvist, J. R. Kitchin, T. Bligaard and H. Jónsson, *J. Phys. Chem. B*, 2004, **108**, 17886–17892.

9 I. T. McCrum, M. A. Hickner and M. J. Janik, *Langmuir*, 2017, **33**, 7043–7052.

10 K. J. Andersson, H. Ogasawara, D. Nordlund, G. E. Brown and A. Nilsson, *J. Phys. Chem. C*, 2014, **118**, 21896–21903.

11 V. H. Y. Chen, G. Mallia, R. Martínez-Casado and N. M. Harrison, *Phys. Rev. B - Condens. Matter Mater. Phys.*, 2015, **92**, 1–9.

12 D. Zherebetskyy, M. Scheele, Y. Zhang, N. Bronstein, C. Thompson, D. Britt, M. Salmeron, P. Alivisatos and L.-W. Wang, *Science*, 2014, **344**, 1380–1384.

13 S. Hamad, S. Cristol and C. R. A. Catlow, *J. Phys. Chem. B*, 2002, **106**, 11002–11008.

14 H. J. Monkhorst and J. D. Pack, *Phys. Rev. B*, 1976, **13**, 5188–5192.

15 Y.-L. Lee, J. Kleis, J. Rossmeisl, Y. Shao-Horn and D. Morgan, *Energy Environ. Sci.*, 2011, **4**, 3966–3970.

16 A. Grimaud, K. J. May, C. E. Carlton, Y.-L. Lee, M. Risch, W. T. Hong, J. Zhou and Y. Shao-Horn, *Nat. Commun.*, 2013, **4**, 1–7.

17 W. Hong, K. A. Stoerzinger, Y.-L. Lee, L. Giordano, A. J. L. Grimaud, A. M. Johnson, J. Hwang, E. Crumlin, W. Yang and Y. Shao-Horn, *Energy Environ. Sci.*, 2017, **10**, 2190–2200.

18 B. Zhao, L. Zhang, D. Zhen, S. Yoo, Y. Ding, D. Chen, Y. Chen, Q. Zhang, B. Doyle, X. Xiong and M. Liu, *Nat. Commun.*, 2017, **8**, 1–9.

19 R. Jacobs, J. Booske and D. Morgan, *Adv. Funct. Mater.*, 2016, **26**, 5471–5482.

20 M. Shao, Q. Chang, J.-P. Dodelet and R. Chenitz, *Chem. Rev.*, 2016, **116**, 3594–3657.

21 Z. Chen, D. Higgins, A. Yu, L. Zhang and J. Zhang, *Energy Environ. Sci.*, 2011, **4**, 3167–3192.

22 I. V. Malakhov, S. G. Nikitenko, E. R. Savinova, D. I. Kochubey and N. Alonso-Vante, *J. Phys. Chem. B*, 2002, **106**, 1670–1676.

23 N. Alonso-Vante, I. V. Malakho, S. G. Nikitenko and E. R. Sa, *Electrochim. Acta*, 2002, **47**, 3807–3814.

24 K. Lee, L. Zhang and J. Zhang, *Electrochem. commun.*, 2007, **9**, 1704–1708.

25 G. A. Tritsaris, J. K. Nørskov and J. Rossmeisl, *Electrochim. Acta*, 2011, **56**, 9783–9788.

26 J. Suntivich, H. A. Gasteiger, N. Yabuuchi, H. Nakanishi, J. B. Goodenough and Y. Shao-Horn, *Nat. Chem.*, 2011, **3**, 546–550.

27 M. Asadi, K. Kim, C. Liu, A. V. Addepalli, P. Abbasi, P. Yasaei, P. Phillips, A. Behranginia, J. M. Cerrato, R. Haasch, P. Zapol, B. Kumar, R. F. Klie, J. Abiade, L. A. Curtiss and A. Salehi-Khojin, *Science*, 2016, **353**, 467–470.

28 W. J. Durand, A. A. Peterson, F. Studt, F. Abild-Pedersen and J. K. Nørskov, *Surf. Sci.*, 2011, **605**, 1354–1359.

29 S. Liu, M. G. White and P. Liu, *J. Phys. Chem. C*, 2016, **120**, 15288–15298.

30 G. A. Tritsaris, Technical University of Denmark (DTU), 2011.

31 H. Ogasawara, B. Brena, D. Nordlund, M. Nyberg, A. Pelmenschikov, L. G. M. Pettersson and A. Nilsson, *Phys. Rev. Lett.*, 2002, **89**, 2761021–2761024.

32 S. Maier, B. A. J. Lechner, G. A. Somorjai and M. Salmeron, *J. Am. Chem. Soc.*, 2016, **138**, 3145–3151.

33 C. J. Cramer, *Essentials of Computational Chemistry Theories and Models*, John Willey & Sons Ltd, Chichester, Second Edi., 2004.

34 J. Rosen, G. S. Hutchings, Q. Lu, S. Rivera, Y. Zhou, D. G. Vlachos and F. Jiao, *ACS Catal.*, 2015, **5**, 4293–4299.

35 D. A. J. Rand, *J. Electroanal. Chem. Interfacial Electrochem.*, 1977, **83**, 19–32.

36 R. T. Downs and M. Hall-Wallace, *Am. Mineral.*, 2003, **88**, 247–250.